Supplementary Material

Ferroelectric Oxide Surface Chemistry: Water Splitting via Pyroelectricity

Arvin Kakekhani[1,2,*] and Sohrab Ismail-Beigi[1,2,3,4]

[1]Department of Physics,
[2]Center for Research on Interface Structure and Phenomena (CRISP),
[3]Department of Applied Physics,
[4]Department of Mechanical Engineering and Materials Science, Yale University,
New Haven, CT 06520, USA

*Corresponding author email: arvin.kakekhani@yale.edu

A. Pseudopotentials

We employ ultrasoft (Vanderbilt) pseudopotentials for the first principles density functional theory (DFT) calculations. The table below provides the parameters describing the pseudopotentials: the reference valence configuration used during its generation and the cutoff radii for each angular momentum channel.

Atom	Reference state	r^s_{cut} (bohr)	r^p_{cut} (bohr)	r^d_{cut} (bohr)
O	$2s^2 2p^4$	1.3	1.3	---
Pb	$5d^{10} 6s^2 6p^2$	2.5	2.5	2.3
Ti	$3s^2 3p^6 3d^2 4s^2 4p^0$	1.8	1.8	2.0
H	$1s^1$	0.8	---	---
Pt	$5d^9 6s^1 6p^0$	2.26	2.324	2.0

B. Supercell details

We perform DFT calculations with plane-wave basis sets and employ a slab geometry with the (001) direction for the surface normal and the polarization axis. A sample c(2×2) supercells is shown in Fig. 1. The c(2×2) structures have in-plane periodicity in the xy plane with a square unit cell with lattice constant 5.459 Å. This value for 2×2 structures is 7.72 Å. We fix the structure of the second, third and fourth atomic layers of PTO on top of the Pt electrode to their bulk values in order to simulate the mechanical boundary conditions appropriate to a thick PTO film: this leads to reasonable computational expenses and sizes of the simulation cells [1,2]. By "bulk values" we mean the appropriate bulk atomic configuration corresponding to the desired out-of-plane polarized state. For the fixed polarization calculations (that are mentioned here in section D) we fix more layers as shown in Fig.1 to ensure that we isolate the effect of polarization from the "pure" effect of the exchange-correlation (XC) functional on the binding energies and our phase diagrams. The reason is that the LDA XC functional predicts polarization of about $60\,\frac{\mu C}{cm^2}$ (less than $90\,\frac{\mu C}{cm^2}$) for bulk PTO, and if only 3 atomic layers are fixed the polarization tends to decrease as we move from the bulk toward the surface. Thus, in order to make sure we isolate out the effect of

polarization from the effect of the XC functional for these calculations we fix more PTO atomic layers (to structure with fixed $90\frac{\mu C}{cm^2}$ polarization) up to the top layer (see Fig. 1). We note that in the case of GGA XC functionals fixing only 3 bulk atomic layers is enough to ensure the polarization propagates almost perfectly up to the surface, but in order to be fully consistent in this part of the figure (2nd row of Fig. 3 in this supplementary material) we fix more layers (up to the surface layer) even for calculations with the GGA XC functionals.

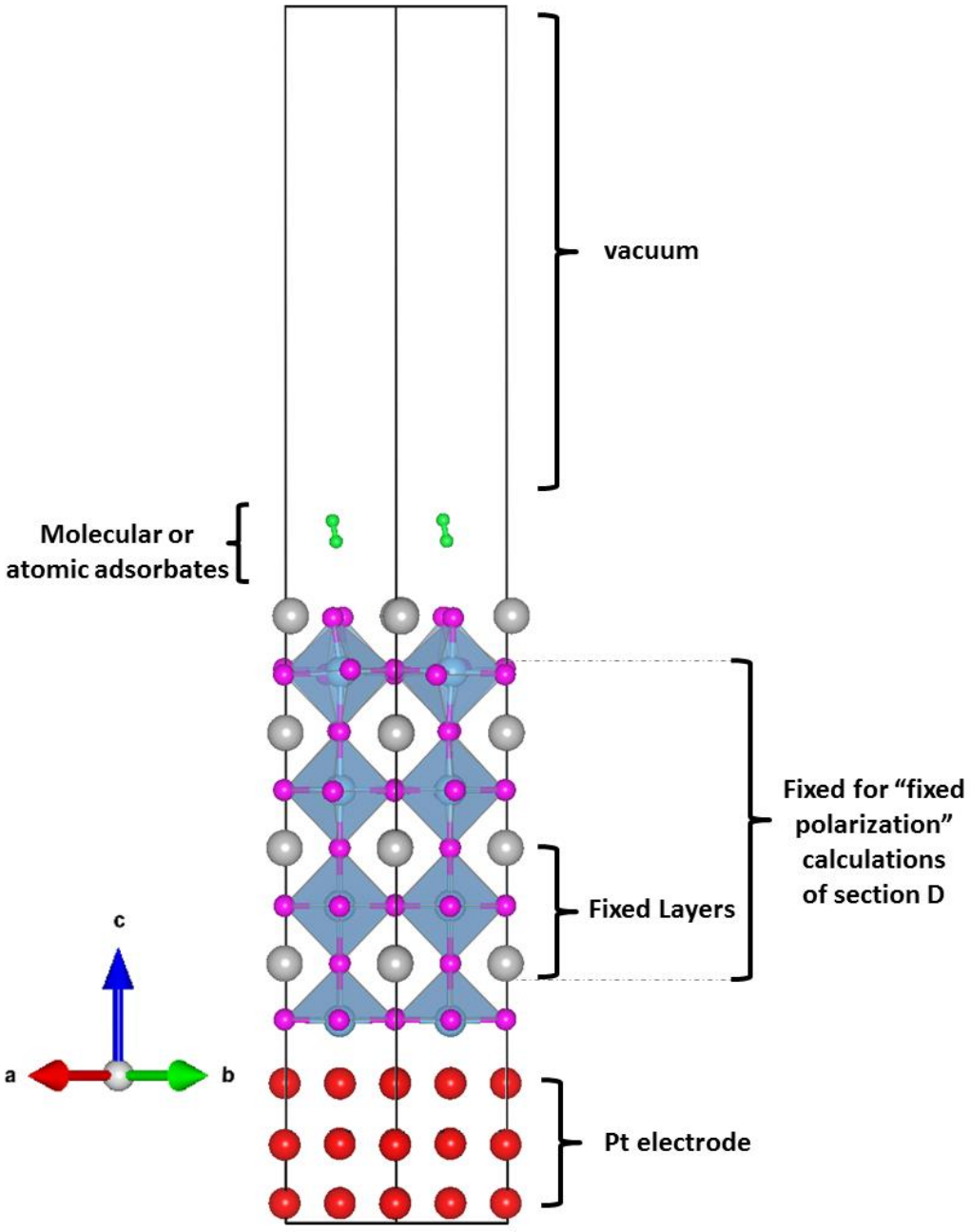

Figure 1) A sample c(2×2) unit cell used in our calculations. Grey balls are Pb, fuchsia balls are O, green balls are H, blue Ti balls are encaged in the blue octahedra formed by the O, and Pt atoms that are used as an electrode at the bottom of the cell are shown in red. Each supercell contains at least 15 Å of vacuum to isolate periodic copies of the slab in z direction.

C. $PbTiO_3$ phase diagrams under varying O and Pb chemical potentials

Compared to prior work [2], the calculations reported in the main text have been improved in two ways: a) more atomic layers near the surfaces have been relaxed which leads to more precise total energies especially for surfaces with vacancies, and b) in **ref.** [2], the O chemical potential was referenced to the theoretically predicted energy of atomic oxygen (half of the theoretically predicted energy of O_2 molecule) plus one-half of the experimental formation energy of O_2, whereas here we use a different reference (fully theoretical energy). The rationalization for the choice in **ref.** [2] was that the resulting phase diagrams would be more experimentally relevant since most DFT calculations produce relatively inaccurate binding energies for molecular O_2. The results here use chemical potentials that are more simply referenced to only theoretical values and are self-consistent within the framework of the DFT calculations.

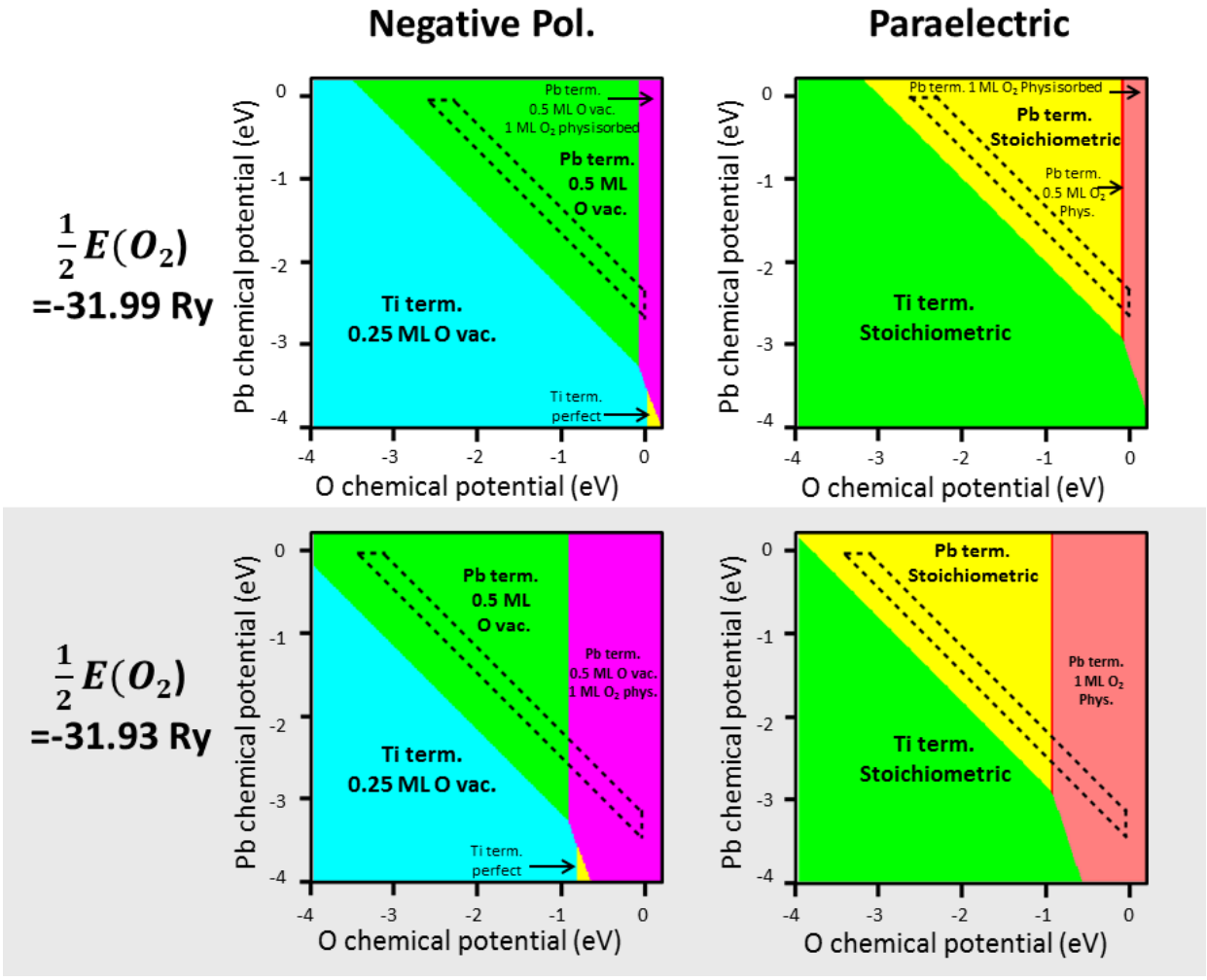

Figure 2) Surface phase diagrams for negatively polarized and paraelectric $PbTiO_3$. In the first row, the oxygen chemical potential is referenced to the fully theoretical DFT value for the energy of oxygen molecule while in the second row, the reference is with respect to the sum of the DFT-derived energy of an oxygen atom and half of the experimental value for O_2 formation energy (i.e., mixed theory+experiment).

The differing consequences of these choices are best explained by example as illustrated in the surface phase diagrams of Fig. 2. The surface phase diagrams generated from the fully theoretical reference chemical potential (first row) would appear more physically sensible and are more consistent with the computed binding energies. For example, one expects the paraelectric surface, due to its insulating nature and lack of mobile electrons or holes, to be chemically inert. Our DFT calculations also predict very weak binding between molecules and this surface: e.g., an O_2 molecule is only weakly physisorbed by 0.2 eV on paraelectric surface. Consistent with this picture, phase diagrams based on fully theoretical value for the O_2 energy reference (first row of Fig. 2) predict that one needs a relatively high oxygen chemical potential to make 0.5 ML of O_2 physisorb on the paraelectric. This is in contrast with the prediction based on the mixed theory+experiment for O_2 energy reference (second row of Fig. 2): apparently, one would need to lower the oxygen chemical potential below -1 eV to desorb the O_2 molecules, which corresponds to an unphysically low pressure of 10^{-20} atm at room temperature [3]. Since correct description of weak physisorption to surfaces is an important part of our catalytic approach, we choose to use the fully theoretical method.

D. Effect of exchange-correlation (XC) functional

As explained above, the results reported in the main text are based on the GGA-PW91 XC functional. In order to check the potential dependence of our key results on the choice of XC functional, we compare our computed surface phase diagrams for three different choices of XC functionals. The resulting surface diagrams are shown in Fig. 3.

As it can be seen in the first row of Fig. 3, LDA-PZ [4], GGA-PBE [5] and GGA-PW91 all predict a stoichiometric phase for the paraelectric case for reasonably accessible ranges of oxygen and water chemical potentials ($-1\ \text{eV} \leq \mu_O, \mu_{H_2O} \leq 0\ \text{eV}$). For a negatively polarized surface in which the magnitude of the out-of-plane polarization in the bulk-like regions of the substrate is fixed to the experimentally observed [6,7] magnitude of P$\approx 90\,\frac{\mu C}{cm^2}$ (2nd row of the figure), all three XC functionals predict very similar phase diagrams (dominated by the phase in which a full monolayer of H atoms cover the surface). What this means is that for a fixed polarization, the different XC approximations do not produce intrinsic binding energies to the surface that differ significantly. For these calculations (2nd row of Fig. 3) we had to fix more than 3 atomic layers (as shown in Fig.1). The reason is that the LDA XC functional predicts polarization of about $60\,\frac{\mu C}{cm^2}$ (less than $90\,\frac{\mu C}{cm^2}$) for bulk PTO, and if only 3 atomic layers are fixed the polarization tends to decrease as we move from the bulk toward the surface. Thus, in order to make sure we isolate out the effect of polarization from the effect of the XC functional for these calculations we fix more PTO atomic layers (to structure with fixed $90\,\frac{\mu C}{cm^2}$ polarization) up to the top layer (see Fig. 1). We note that in the case of GGA XC functionals fixing only 3 bulk atomic layers is enough to ensure the polarization propagates almost perfectly up to the surface, but in order to be fully consistent in this part of the figure (2nd row of Fig. 3) we fix more layers (up to the surface layer) even for calculations with the GGA XC functionals.

In the 3rd row of Fig. 3, we see that the phase diagram that the LDA-PZ XC functional predicts is different from the GGA XC functionals. The root of the difference is because the predicted bulk ferroelectric polarization magnitudes differ between the functionals: the GGAs overestimate ($P \approx 120\ \frac{\mu C}{cm^2}$) while LDA underestimates ($P \approx 60\ \frac{\mu C}{cm^2}$). Hence, the main determinant of the nature of the phase diagram is the magnitude of the bulk polarization which should be well reproduced by the theoretical approach, or if the XC functional it not good enough, it should be fixed "by hand"; the actual binding energies to the surface are far less sensitive to the choice of XC functional.

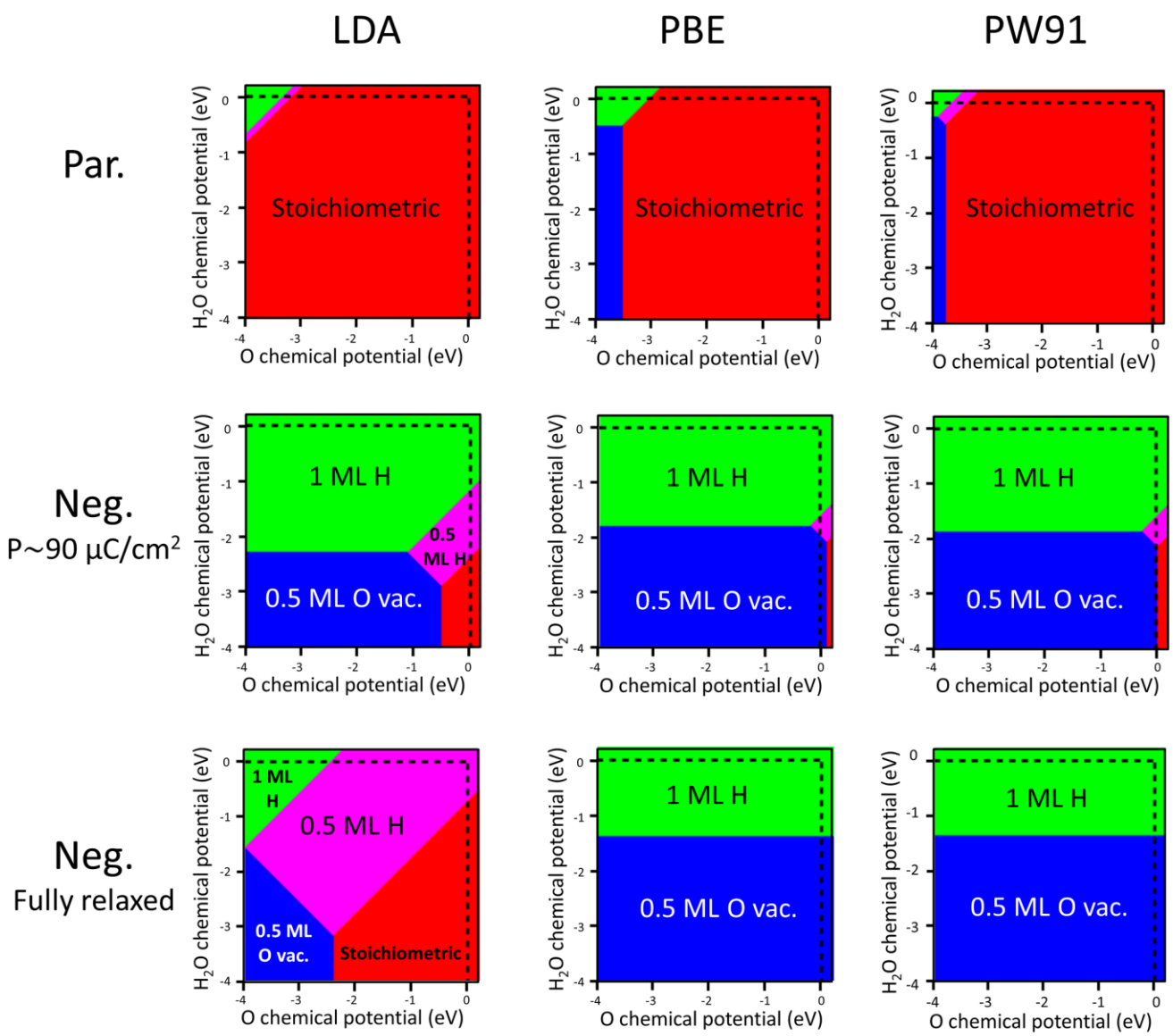

Figure 3) Surface phase diagrams calculated for paraelectric (1st row) and negatively polarized (2nd and 3rd row) substrates using different exchange-correlation (XC) functionals: LDA-PZ (1st column), GGA-PBE (2nd column) and GGA-PW91 (3rd column). The phase diagrams in the 3rd row are based on fully relaxed calculations for negative polarization, while the phase diagrams in the 2nd row are based on calculations in which the interior atomic layers of the ferroelectric are fixed to produce a specific polarization of P≈90 $\frac{\mu C}{cm^2}$ but the surface layer is free to relax. Comparing the second and third row clarifies the XC-dependent effect of the bulk polarization as opposed to the surface binding energies.

E. Energetics and atomic coordinates for the structures used in this work regarding the hydrogen production cycle

The absolute energies computed by DFT (GGA-PW91 XC) for structures and molecules that are involved in the catalytic cycle depicted in the paper are given in the table below:

Structure, atom or molecule	Total Energy (Ry)
Bare negatively poled PTO surface (2×2)	-7491.2091
Transition state of O_2 forming on neg. surface (2×2)	-7491.1814
Negatively poled PTO surface with 0.5 ML O vac. c(2×2)	-3713.679
Negatively poled PTO surface with 0.5 ML O vac. (2×2)	-7427.3283
O_2 on negatively poled PTO with 0.5 ML O vac. (2×2)	-7491.3000
Negatively poled PTO surface with 1 ML H c(2×2)	-3748.2853
Paraelectric PTO surface with 1 ML H c(2×2)	-3748.0499
Transition state of H_2 forming on paraelectric surface c(2×2)	-3748.0292
H_2 on paraelectric surface c(2×2)	-3748.1010
Bare paraelectric surface c(2×2)	-3745.7603
H_2 (in a big box, i.e., in gas)	-2.3377
H (in a big box, i.e., in gas)	-0.9202
O_2 (in a big box, i.e., in gas)	-63.9792
OH (in a big box, i.e., in gas)	-33.0628
H_2O (in a big box, i.e., in gas)	-34.5066

Below are the important energy barriers involved in the catalytic cycle depicted in the paper:

Process	Energy Barrier (eV)
O_2 formation barrier on negatively poled surface	0.4
H_2O dissociation on negatively poled 0.5 ML O vac. surface	0.0
H_2 formation barrier on paraelectric surface	0.3
O_2 desorption barrier from 0.5 ML O vac. surface	0.0
H_2 desorption from paraelectric surface	0.0

References (for Supplementary Material)

(1) Kakekhani, A., Ismail-Beigi, S. ACS Catalysis, 2015, 5 (8), pp 4537–4545

(2) Garrity, K., Kakekhani, A., Kolpak, A. and Ismail-Beigi, S. Physical Review B 88.4 (2013): 045401.

(3) Kolpak, A., Ismail-Beigi, S. Physical Review B 83, no. 16 (2011): 165318.

(4) Perdew, John P., and Alex Zunger. Physical Review B 23.10 (1981): 5048.

(5) Perdew, John P., Kieron Burke, and Yue Wang. Physical Review B 54.23 (1996): 16533.

(6) Morioka, Hitoshi, et al. Applied physics letters 82.26 (2003): 4761-4763

(7) Morita, Takeshi, and Yasuo Cho Japanese journal of applied physics 43.9S (2004): 6535